



Photocatalytic recovery of H₂ from H₂S containing wastewater: Surface and interface control of photo-excitons in Cu₂S@TiO₂ core-shell nanostructures

V. Navakoteswara Rao^a, N. Lakshmana Reddy^a, M. Mamatha Kumari^a, P. Ravi^b, M. Sathish^b, K.M. Kuruvilla^c, V. Preethi^{c,**}, Kakarla Raghava Reddy^d, Nagaraj P. Shetti^{e,f}, Tejraj M. Aminabhavi^{f,g,*}, M.V. Shankar^{a,**}

^a Nanocatalysis and Solar Fuels Research Laboratory, Department of Materials Science & Nanotechnology, Yogi Vemana University, Kadapa, Andhra Pradesh, 516005 India

^b Functional Materials Division, Central Electrochemical Research Institute (CSIR-CECRI), Karaikudi, Tamil Nadu, 630003 India

^c Department of Civil Engineering, Hindustan Institute of Technology and Science, Padur, Chennai, Tamil Nadu, 603103 India

^d School of Chemical and Biomolecular Engineering, The University of Sydney, Sydney, NSW 2006, Australia

^e Electrochemistry and Materials Group, Department of Chemistry, K. L. E. Institute of Technology, Gokul, Hubballi-580030, Affiliated to Visvesvaraya Technological University, Karnataka, India

^f Department of Chemistry and Biochemistry, Lamar University, Beaumont, Texas 77710, USA

^g SET's College of Pharmacy, Dharwad, Karnataka, 580002 India

ARTICLE INFO

Keywords:

Core-shell structure
Shell thickness
Hydrogen production
Sulphide wastewater
Inorganic sacrificial agent
Apparent
Quantum efficiency

ABSTRACT

This study focuses on the synthesis of Cu₂S particles as the core wrapped-up with thin layer of TiO₂-shell for improved surface and interface control of photo-excitons for H₂ production. Chemical states of metal Cu⁺, Ti⁴⁺ ions were confirmed by X-ray Photo-electron and Electron Paramagnetic Resonance (g-factor of 2.03) Spectroscopy. Transmission Electron Microscopic images revealed the hexagonal shape of Cu₂S wrapped-up with TiO₂ having the shell thickness varying from 12.0 to 16.7 nm. Time resolved transient photoluminescence decay spectra confirmed that three folds prolonged life-time of excitons generated on Cu₂S@TiO₂ core-shell than pristine Cu₂S. The batch photo-reactor used to evaluate the performance of photocatalysts in an aqueous solution containing Na₂S/Na₂SO₄ promoted oxidation reaction for H⁺ generation. The control over shell thickness directly influenced the optical and surface-interface properties, resulting in the enhanced H₂ production of 41.6 mmol h⁻¹ g⁻¹ of catalyst for an optimized catalyst with UV-vis light to H₂ production efficiency of 10.3%. The same catalyst also exhibited excellent stability for un-interrupted H₂ production upto 30 h, along with good results on recyclability and reusable efficiency. Scale-up operation performed to recover H₂ from sulphide wastewater in tank photo-reactor triggered H₂ gas 16.1 mmol h⁻¹ g⁻¹ of catalyst.

1. Introduction

Hydrogen (H₂) fuel production via photocatalytic process by utilizing solar light is considered as a simple, sustainable and renewable route. This process often works well under ambient conditions and produces H₂ via detoxifying industrial wastewater, which ensures the environmental cleaning and energy production is a novel approach to reform industrial waste [1,2]. Sulfide ions present in industrial wastes either as S²⁻ or hydrogen sulfide (H₂S) are toxic having an unpleasant odor. Petrochemical industry releases H₂S containing (15–20%) wastewater as a by-product, and their treatment process produces elemental sulfur. Also, sewage treatment plant releases the wastewater

containing sulphide ion with concentration greater than 1200 mg/L. At present a large amount of energy being spent for this treatment, whereas photocatalytic process can be effectively utilized to recover H₂ gas [3,4].

The H₂ generation can be obtained using a variety of nanohybrid materials such as those including, but not limited to semiconductor metal chalcogenides [5–7]. And also a few reports on N-doped metal oxides, metal chalcogenides [7–11], noble metals as co-catalyst as well as core-shell co-catalyst [12–15], transition metal oxides [16–18], mixed metal oxides [19,20], metals as a co-catalyst [21,22], bimetallic quantum dot nanocomposites [23,24], transition metal chalcogenides [25,26]. A variety of metal oxides have also been used for H₂S splitting

* Corresponding author at: SET's College of Pharmacy, Dharwad, Karnataka, 580002 India.

** Corresponding authors.

E-mail addresses: vpreethi@hindustanuniv.ac.in (V. Preethi), aminabhavit@gmail.com (T.M. Aminabhavi), shankar@yogivemanauniversity.ac.in (M.V. Shankar).

such as noble metal and metal oxides [27,28], and metal and metal oxides/ sulphides [29]. However, their efficiency is still low to claim for large-scale applications. Recently our group reported, metal chalcogenide based core-shell type photocatalysts have attracted much interest to improve efficiency and suppressed the photo-corrosion [30–32]. Especially, Cu₂S based core-shell materials are attractive in view of their tunable optical and catalytic properties.

Copper is an earth-abundant material and Cu₂S synthesized by using simple chemical method having better semiconducting properties to absorb solar light and hence it is potential material for photocatalytic H₂ generation. It was explained that Cu₂S have narrow band gap from 1.8 to 2.4 eV, have the potential to absorb visible spectrum of solar light and generated excitons have required potential for oxidation and reduction reactions [33,34]. All these attributes favor Cu₂S to be a potential photocatalyst for H₂ production, but photo-corrosion in Cu₂S is a bottle-neck to scale-up. Hence, construction of core-shell type materials is considered to be a viable opportunity to overcome these issues. Titania is a well-known UV light active photocatalyst with exceptional properties such as non-toxicity, low cost, low infrared absorption, good photo-stability, transparency under UV-vis light, suitable band edge potential and catalytic active sites [35]. It is considered as one of the promising materials for the photocatalytic splitting of water into O₂ and H₂ gases [36]. It is expected that the combination of the two best photocatalysts (Cu₂S, TiO₂) can be a suitable approach to improve the overall photocatalytic efficiency.

In the earlier literature, Park et al., reported Cu₂S spherical type nanostructures decorated with metal as a co-catalysts for H₂ generation [37]. Kar et al., reported the synthesis and properties of Cu₂S, CuS nanorods and nanowalls for CO₂ photoreduction [38]. Low-thermal synthesis of CuS quantum dots decorated on TiO₂ nanotube was also reported [39]. The role of co-catalyst in CuS@TiO₂ core-shell structured particle has been studied [40]. CuS nanorods, as well as nanowires, were synthesized by the simple chemical method by Poulomi Roy et al. [41]. Non noble-metal CuS-CdS nanocomposites were evaluated for photocatalytic H₂ production [42]. Cu₂S nanostructures with different morphologies such as 2-D hierarchical, nanobelts, nanorod, and nanowires were also reported [43–45]. To the best of our knowledge, no reports on Cu₂S@TiO₂ based core-shell materials for photocatalytic H₂ generation. Hence, in this study, we synthesize Cu₂S@TiO₂ core-shell materials by a two-stage method using structure-directing agent, resulting in uniformly coated core-shell nanostructures with a shell thickness of few nanometres. Experimental parameters were fine-tuned to attain higher catalytic activity of 41.6 mmol h⁻¹ g⁻¹ of catalyst besides continuous H₂ generation (time-on-stream) for 30 h. The optimized catalyst used in tank photo-reactor to recover H₂ gas from sulphide containing wastewater and showed enhanced H₂ generation rate of 16.1 mmol h⁻¹ g⁻¹ of catalyst.

2. Experimental section

2.1. Design and synthesis of core-shell photocatalyst

A simple two-step process was designed for synthesis of hierarchical core-shell morphology of Cu₂S@TiO₂ photocatalyst. At first, core material containing Cu₂S particle was prepared using structure-directing agent and followed by hydrothermal treatment.

2.1.1. Preparation of Cu₂S particles

Hydrothermal method and parameters were adopted from recent report [44]. Herein, 1:2 mol ratio of copper chloride di-hydrate (2.72 g, 0.53 M) and thiourea (2.43 g, 1.06 M) were sequentially added into ethylene diamine (30 mL) under magnetic stirring (15 min) at 30 ± 2 °C. The resulting mixture (pH = 13.5 ± 0.2) was packed and sealed in an autoclave and heated in electric oven at 180 °C for 6 h. Thus the precipitate was collected via centrifugation and subjected to washing twice with distilled H₂O followed by C₂H₅OH. Finally, black

material was dried at 80 ± 2 °C for 12 h and labelled as Cu₂S. The same procedure was repeated few times to collect few grams of catalyst used for characterization and photocatalytic activity.

2.1.2. Preparation of Cu₂S@TiO₂ core-shell morphology

A surface protection thin-layer of TiO₂ on Cu₂S particles was achieved by following the experimental conditions reported in recent publication [46]. Typically, 1:0.3 M ratios of Cu₂S particles (50 mg) and trisodium citrate dihydrate (200 mg) was sequentially added into 50 mL of iso-propanol subjected to sonication for 30 min at 30 ± 2 °C. An amount of Ti[OCH(CH₃)₂]₄ (TTIP, 0.42 mL) solution was drop-wise added into the above suspension containing Cu₂S, followed by drop-wise addition of deionized H₂O (30 mL) and stirring continued for 2 h at 30 ± 2 °C. The above mixture was transferred and sealed in an autoclave, which then heated at 180 ± 2 °C for 15 h. The black product washed twice in deionized H₂O followed by C₂H₅OH, centrifuged to separate the solid and dried at 80 ± 2 °C for 12 h. In order to study the effect of shell thickness (TiO₂) the concentration of TTIP varied from 0.14, 0.28, 0.42, 0.59 and 0.74 mL (0.01M to 0.08M) which are labelled as CST-1, CST-2, CST-3, CST-4 and CST-5 respectively. The same procedure was repeated few times to collect few grams of catalyst used for characterization and photocatalytic activity.

2.2. Photocatalytic hydrogen production

2.2.1. Batch photo-reactor

The detailed experimental procedure is elaborated in recent report [31]. In brief, known amount of chosen photocatalyst was dispersed into aqueous solution of Na₂S and Na₂SO₄ (0.3 M, 50 mL) kept in single port quartz photo-reactor (190 mL). The reactor port was tightly sealed with rubber septum and the contents were subjected to adsorption and nitrogen gas purging results in inert conditions. A solar simulator (Xe lamp = 260 W, Oriel Instruments, Newport Corporation, USA) fitted with infra-red filter used to carryout photocatalytic experiments. The entire set-up kept in air-conditioned facility and maintained experimental temperature of 25 ± 2 °C. At periodic interval of one hour, gas samples withdrawn using gas syringe from the photo-reactor injected into gas chromatograph (Shimadzu Gas Chromatograph-2014) fitted with a thermal conductivity detector. All the gas samples were analysed at identical experimental conditions.

2.2.2. Tank photo-reactor

Fig. 1 shows the photographic image of square shaped tank photo-reactor (capacity 5 L) made-up of acrylic plastic used in the present experimental work. Reactor consists of two cylindrical type tubes, the first one used for N₂ gas purging, and other one used to collect the H₂ gas generated through photocatalytic process. The sulphide wastewater collected from biogas scrubbing unit, a sewage treatment plant (STP) and its sulphide concentration (1280 mg/L) was analyzed by the standard iodometric method. Prior to solar light irradiation, the reactor purged with N₂ gas for 45 min to ensure the inert atmosphere and adsorption under dark condition. The generated H₂ gas was quantified by water displacement method using inverted measuring cylinder. The photocatalytic experiments were carried out under solar light irradiation at Padur, Chennai, India (location 12.48 °N 80.13 °E) the light intensity was measured every hours using a Lux meter (Model: LX 101A) between 10.00 a.m. to 2.00 pm and average light intensity is about 86,800lx.

3. Results and discussion

3.1. Steps involved in synthesis of Cu₂S@TiO₂ core-shell

Fig. 2 illustrates the step-wise formation of Cu₂S@TiO₂ core-shell by a facile double stage method. At first, preparation of Cu₂S core (i) Dissolution of copper precursor in ethylene diamine solution (served as

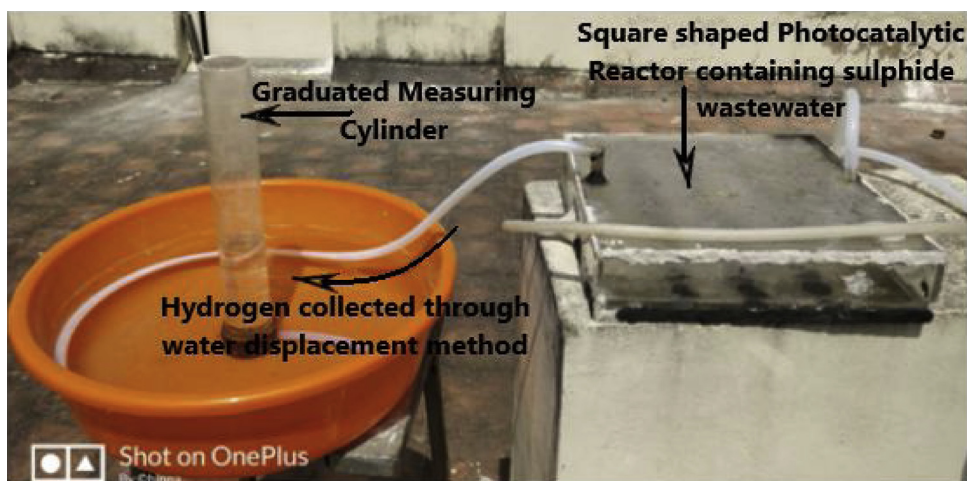


Fig. 1. Experimental set-up for the photocatalytic recovery of H_2 from H_2S containing industrial wastewater under solar light irradiation.

structure-directing agent) turns colourless into blue colour indicates copper ions attached to ethylene diamine (en) in the form of $Cu(en)_2$. (ii) Addition of thiourea results change of colour from blue to pale green due to formation of surface urea complex. (iii) Upon continuous magnetic stirring thus obtained black Cu_2S adsorbed with reaction by-products on hexagonal and spheroids morphologies. (iv) Hetero-structures of hexagonal and spheroids shapes with negative surface charge obtained. Secondly, preparation of thin-layer of TiO_2 shell (v) a positive ion layer formed on Cu_2S particles by dispersion in tri-sodium citrate solution. (vi) TTIP hydrolyzed to form $Ti(OH)_4$ anions in-turn adsorbed on positive layer of Cu_2S (vii) a thin-layer of TiO_2 formed on Cu_2S besides adsorption of reaction by-products. (viii) dried material have clean surface of $Cu_2S@TiO_2$ core-shell structure.

3.2. Characterization of photocatalysts

3.2.1. Structural and morphological analysis

Fig. 3 shows XRD pattern of pristine and core-shell photocatalysts with different TiO_2 amount. The cuprous sulfide showed cubic crystal and chalcocite phases, that match with the standard JCPDS values. The 2θ values located at 27.9, 29.4, 32.3 and 46.4° are correlated with (100), (111), (200) and (220) planes of Cu_2S [44,48]. The peak at $2\theta = 25.42^\circ$ indicates (101) plane of TiO_2 anatase phase (JCPDS No: 21-1272) with tetragonal crystal structure. These values are in good agreement with $Cu_2S@TiO_2$ core-shell nanocomposites [49,50]. In Fig. 3, one can see that with increasing the concentration of TTIP leads to increased TiO_2 content onto the surface of the core (Cu_2S), the peak intensities

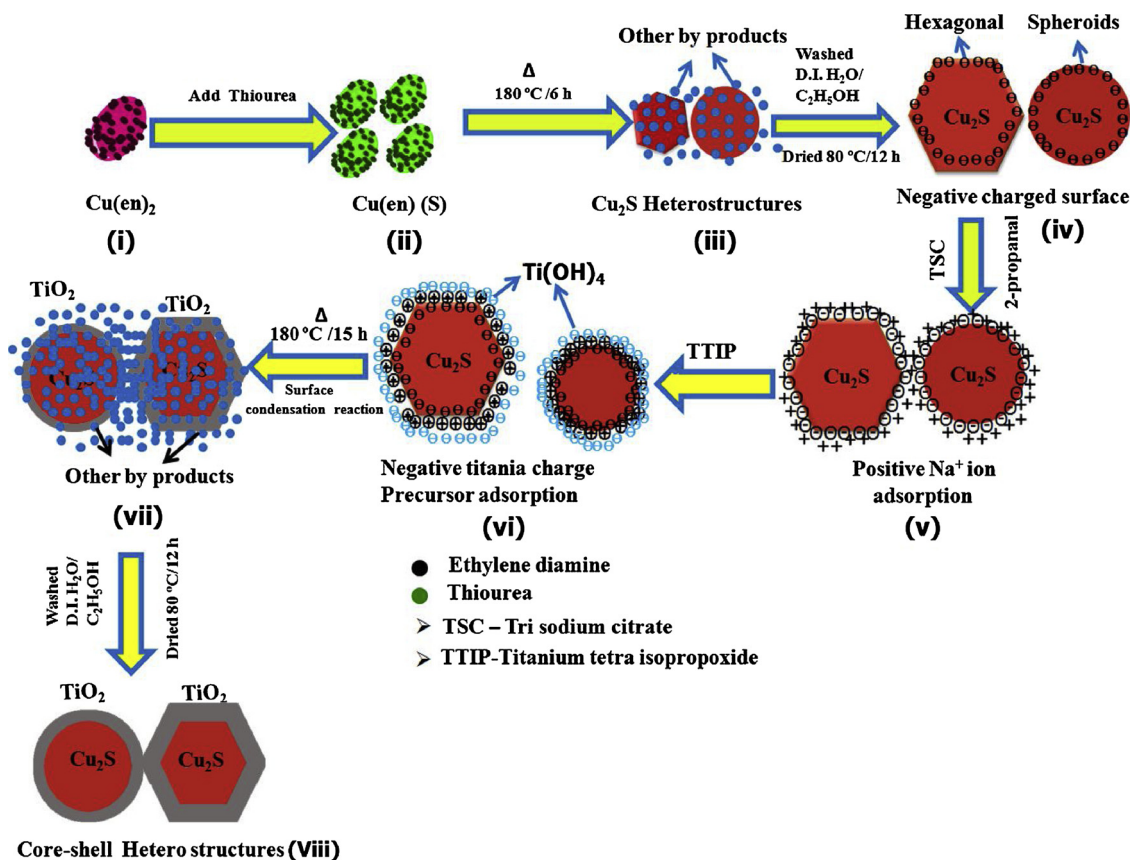


Fig. 2. Schematic illustration of $Cu_2S@TiO_2$ core-shell nanostructures in two-step method.

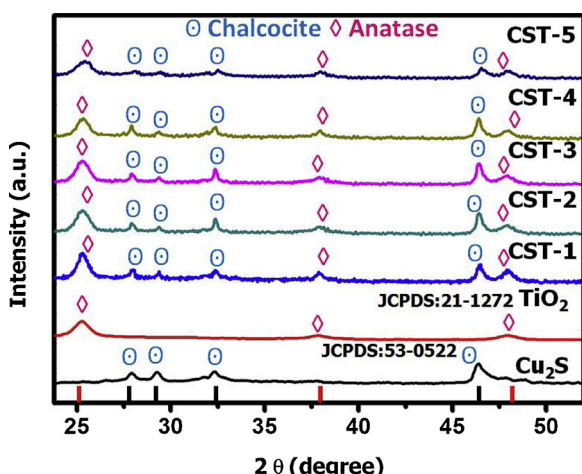


Fig. 3. XRD pattern of pristine and $\text{Cu}_2\text{S}@\text{TiO}_2$ core-shell photocatalysts.

decrease from CST-1 to CST-5 compared to the crystallinity of TiO_2 . Recently, Li et al., [49] reported $\text{Cu}_2\text{S}@\text{ZnO}$ hetero nanostructures and explained about the crystal structure as well as phase. Xue et al., explained the crystal planes and phase corresponds to Cu_2S for Li-ion batteries [44]. Their result denotes that the synthesis time may also improve the purity and phase structure of the final core-shell structure.

FT-IR spectrum of CST-3, pristine TiO_2 and Cu_2S photocatalysts displayed in Fig. FS1 show strong peaks at 1085 and 1040 cm^{-1} that are assigned to stretching vibration of Cu-S in Ti-O group in $\text{C}_2\text{H}_5\text{OH}$. The peak at 890 cm^{-1} assigned to Ti of CST-3, while peaks of pristine Cu_2S and TiO_2 were well matched with stretching frequency values of CST-3 core-shell nanocomposites. The spectra of pristine TiO_2 , Cu_2S and CST-3 are consistent with standard spectra of TiO_2 and Cu_2S [51,52]. The O-H stretching vibrations observed at 3445 cm^{-1} indicate OH functional group present in $\text{Cu}_2\text{S}@\text{TiO}_2$ core-shell is ascribed to moisture present of the composite. Absorption at 1626 cm^{-1} corresponds to Cu_2S stretching in S group, while a shoulder peak at 1612 cm^{-1} is due to sulfur and double bond bending. The peak around 1145 - 1350 cm^{-1} corresponds to oxygen and Cu^{+1} stretching, while those at 632.5 and 634.5 cm^{-1} are assigned to $\delta\text{-Ti}^{+4}$. The above results show well separated and intense peaks confirming no impurities of the core-shell material [51,53,54].

Fig. 4 shows TEM images of Cu_2S and $\text{Cu}_2\text{S}@\text{TiO}_2$ core-shell (CST-2, CST-3 and CST-4) photocatalysts. Fig. 4(a) display hetero nanostructures predominantly with a hexagonal structure. The pristine Cu_2S has an average diameter of 336 nm and core Cu_2S is protected by the nanoscale layer of anatase TiO_2 uniform shell (Fig. 4 (b,c)). The structures have hexagonal nanosheet-like morphology with a length about 603 nm . For the core, average diameter was 331 nm and TiO_2 shell thickness increased at higher mole concentration of TiO_2 precursor. The shell thicknesses of CST-2, CST-3 and CST-4 are 12.04 , 13.2 , and 16.7 nm , respectively (shown in Fig. 4(c, d, f)). HR-TEM image of CST-3 catalysts displayed lattice fringe of $d = 0.307\text{ \AA}$, suggesting the existence of (110) plane of Cu_2S and the coated shell layer showed existance of anatase TiO_2 with $d = 0.354\text{ \AA}$ correspondindg to (101) plane (Fig. 3e). Fig. 3 (g) revealed the elemental composition of Ti (10%), Cu (46%), S(23%) and O (21%) in optimized CST-3 hierachical nanocomposite (Fig. 4f). Further consolidated elemental mapping of the CST-3 core-shell photocatalyst shown in Fig. FS2(a). Fig. FS2(b-d) depicts mapping of individual elements copper, sulphur, titanium and oxygen and it confirms the uniform distribution in the photocatalyst.

3.2.2. Optical and surface properties of $\text{Cu}_2\text{S}@\text{TiO}_2$ photocatalyst

The UV-vis spectrum of core-shell photocatalysts are displayed in Fig. 5. It shows two shoulder-peaks, of which one is assigned to UV-light absorption in the range of 395 – 405 nm attributed to light absorption by

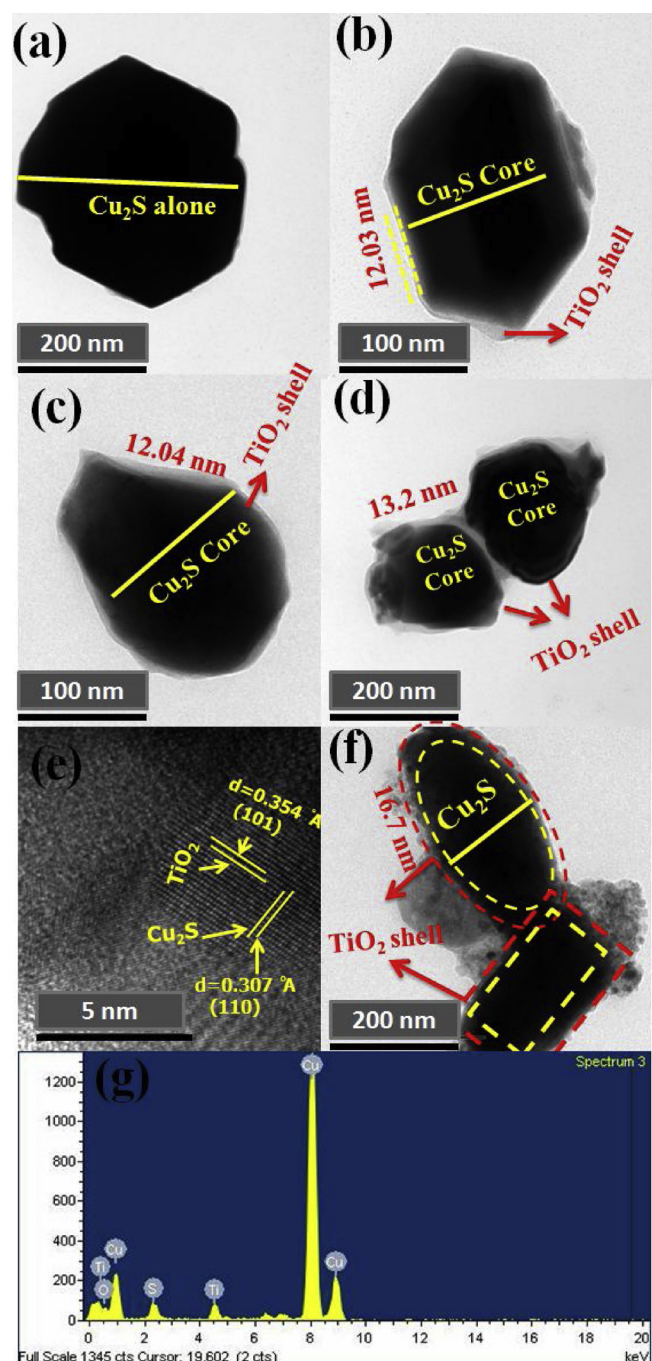


Fig. 4. HR-TEM images of $\text{Cu}_2\text{S}@\text{TiO}_2$ core-shell photocatalysts (a) Cu_2S hexagonal particle (b,c) Shell thickness of CST-2 (d) Shell thickness of CST-3 (e) SAED pattern of CST-3 (f) Shell thickness of CST-4 (g) EDAX of CST-3.

TiO_2 , while the second peak between 550 and 555 nm assigned to Cu_2S core material which indicates cuprous sulfide allows visible light absorption region. The relative intensity of cuprous sulfide with respect to the core material decreases, however, the absorption edge shifted towards 550 – 620 nm with increasing the amount of TiO_2 from CST-1 to CST-5. The decrease in visible absorption spectrum is proportional to amount of TiO_2 precursor that fetched thicker layer which contributes to reflection of irradiated light [55–57]. The absorption of Cu_2S and $\text{Cu}_2\text{S}@\text{TiO}_2$ catalysts around 620 nm is ascribed to absorption of visible light by Cu_2S [58] while the core-shell catalyst absorbs both in UV-vis and visible light due to the combination of narrow (Cu_2S) and wide band gap (TiO_2) materials [59,60].

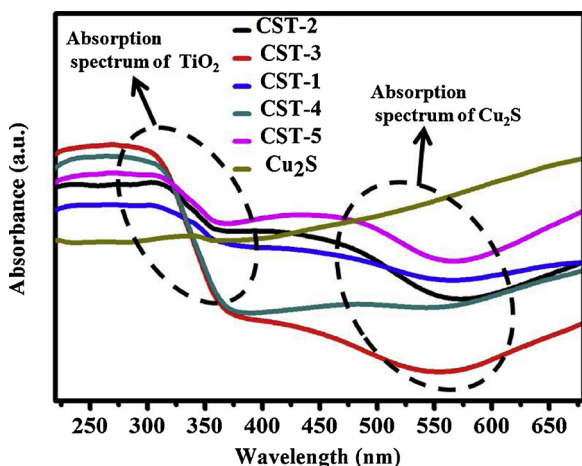


Fig. 5. DR UV-vis spectra of Cu_2S and $\text{Cu}_2\text{S}@\text{TiO}_2$ core-shell photocatalysts.

Fig. 6 shows the X-ray photoelectron spectrum of CST-3. The Cu 2p peak in Fig. 6(a) shows two major peaks at 931.8 and 951.7 eV attributed to Cu 2p_{3/2} and Cu 2p_{1/2} and shake up peak are present in the core-shell composites which conforms copper exhibits +1 oxidation state. Fig. 6(b) displays S 2p spectrum, with major peaks at 161.8 and 160.6 eV, respectively that correspond to S 2p_{1/2} and S 2p_{3/2}, where sulfur exists as S^{2-} . The binding energy values of copper (Cu) and sulphur (S) are in good agreement with the earlier studies [25,61,62]. Fig. 6(c) depicts two peaks one at 457.3 and another at 463.3 eV that are attributed to 2p_{3/2} and 2p_{1/2} of Titanium exists Ti^{4+} state. The peaks at 528.4 and 530.5 eV corresponding to O 1s spectra reveal the existence of O^{2-} valence state (Fig. 6(d)). The binding energy values of

Ti, O, Cu and S in the optimized catalyst well matched with the standard values and are in their stable oxidation states and well correlate with the literature reports [63,64].

Electronic paramagnetic resonance spectroscopy (EPR) analysis provided information on the characteristic atomic state of the compositions and electronic structure of $\text{Cu}_2\text{S}/\text{TiO}_2$ core-shell and pristine Cu_2S materials. Fig. 7 (a and b) shows EPR spectrum of $\text{Cu}_2\text{S}@\text{TiO}_2$ and Cu_2S photocatalyst showed singlet signal and g-factor value of 2.03. The results are in good agreement with literature value and confirm that copper exists as +1 and titanium has +4 oxidation states in CST-3 photocatalyst [65,66].

3.2.3. Life-time studies of photo-excitons

Fig. 8(a) displayed the photoluminescence (PL) spectra of pristine and core/shell photocatalysts. The experimental data on wavelength versus peak intensity shows that the peak intensity of CST-3 is significantly lower than Cu_2S . Under identical conditions, the peak intensity describes the recombination rate of photo-excitons thus hierarchical structure in core/shell CST-3 showed lower rate of recombination [67]. In order to explore the life-time of photo-excitons, time-resolved emission spectra were recorded at 428 nm for both catalysts and results as time versus peak intensity is displayed in Fig. 8(b). The emission decay kinetics for Cu_2S and CST-3 fitted single-exponentially with time constants (τ) 24.5 and 92.9 Ps respectively. It is interesting to note that photo-excitons in CST-3 have more than 3 folds prolonged life-time than Cu_2S alone. The spatial separation of electron and hole in excitons result in decrease of wave function overlap and thus a longer lifetime in type II heterostructures. As a result, increase in life-time of charge carriers in core-shell can be explained in two ways, an effective spatial separation of excitons via band bending from Cu_2S to TiO_2 surface and secondly trapping at defects located at interface. Recent report on CdSe-ZnS core-shell quantum dots bonded cobalt

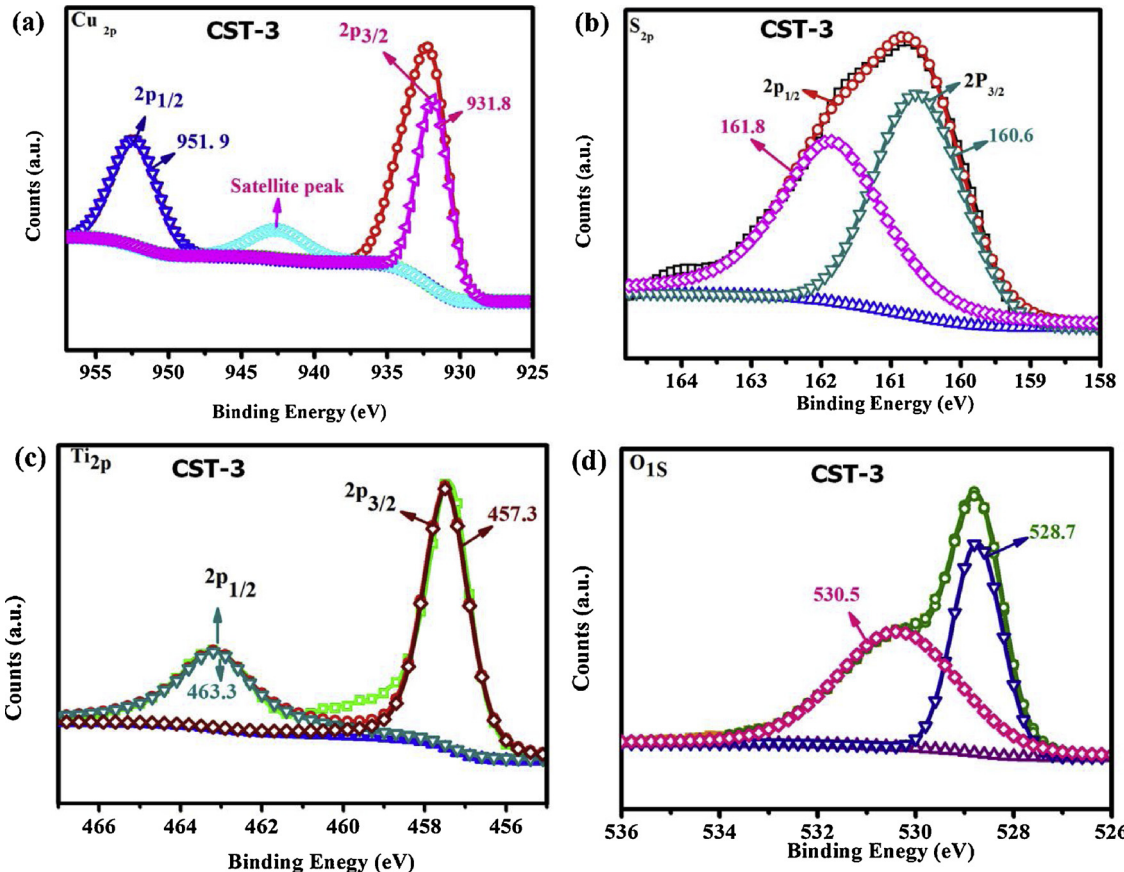
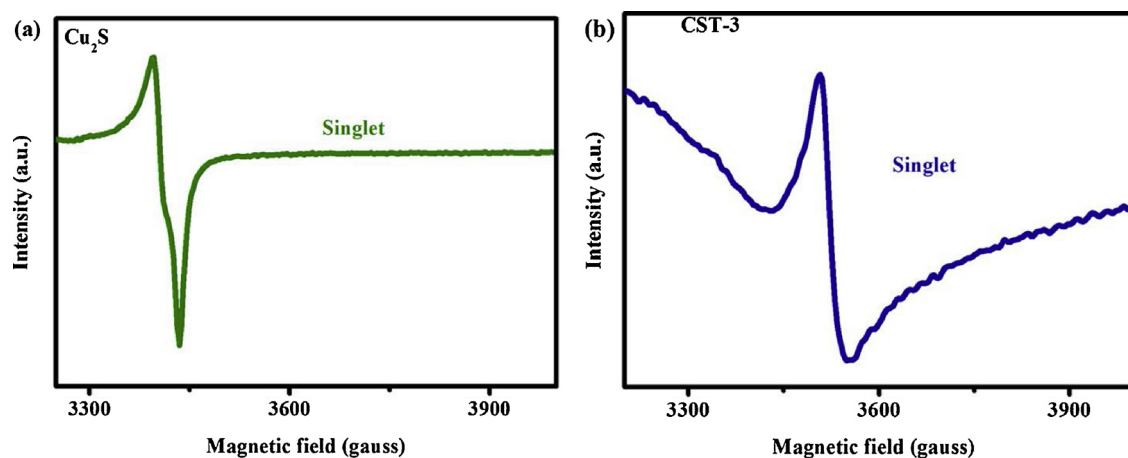
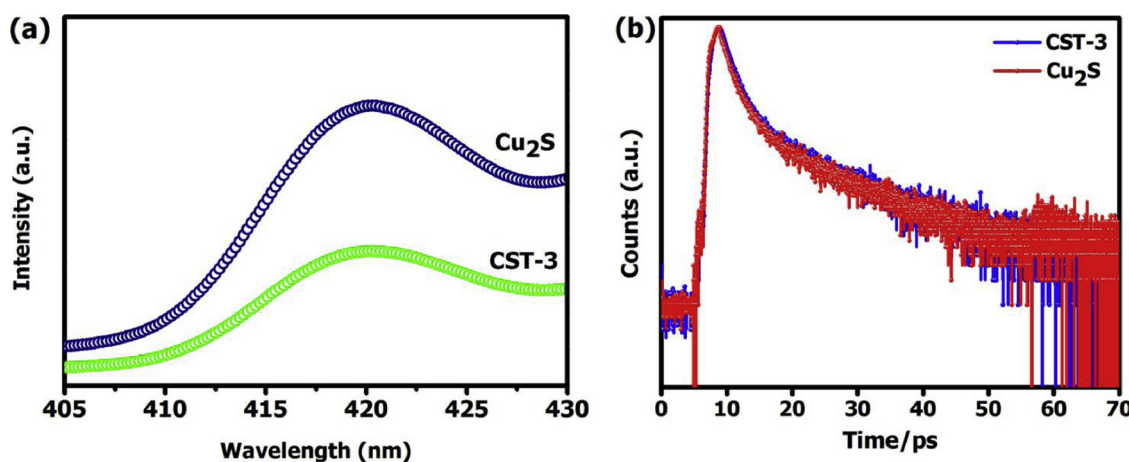


Fig. 6. X-ray photoelectron spectroscopy of CST-3 core-shell photocatalyst (a) Cu 2p (b) S 2p (c) Ti 2p (d) O 1s.

Fig. 7. Electronic spin resonance spectra of (a) Cu₂S (b) CST-3 core-shell photocatalysts.Fig. 8. (a) Photoluminescence decay spectra (b) Time resolved photoluminescence decay spectra of Cu₂S and CST-3 core-shell photocatalyst.

complexes at different concentration QD-C₁, QD-C₂ and QD-C₃ showed a time resolved life time of 6.99–20.51 ns and 3.39 ns for pristine material [68]. Rawalekar et al. [69], elaborated prolonged life-time of charge carries in CdTe-CdS ($\tau = 27.6$ ns) core-shell nanostructures than CdTe ($\tau = 2.12$ ns).

3.3. Photocatalytic H₂ generation in batch reactor under simulated solar light irradiation

In core-shell type of photocatalysts, shell thickness plays predominant role for effective transmittance of light into semiconductor particle kept inside core available for photo-excitation process [32,70]. Similarly, exciton migrates from core to shell surface with life-time of few nanoseconds that involves in-situ redox reactions with molecules adsorbed at catalytic active sites. Hence, core protects the shell for direct contact with reaction medium. Often, core plays photo-sensitizer role and shell acts as catalyst/co-catalyst for surface reactions. In order to achieve improved H₂ generation and photon utilization efficiency optimization of shell thickness as well as type of sacrificial agents are mandatory [23,71].

3.3.1. Effect of TiO₂ shell thickness in Cu₂S@TiO₂ photocatalysts

Core-shell photocatalyst, Cu₂S@TiO₂ with five different shell-thicknesses were studied for photocatalytic H₂ generation with aqueous solution containing (0.3 M) Na₂S and Na₂SO₄. The experiments were carried out under simulated solar light irradiation for 4 h and the rate of H₂ generation was calculated using standard formula for per hour and one gram catalyst. Fig. 9(a) displays rate of photocatalytic H₂

generation by using core-shell with variable shell thickness and pristine catalysts in the following order CST-3 > CST-4 > CST-2 > CST-5 > CST-1 > Cu₂S > TiO₂. Among them, CST-3 shows highest rate of H₂ generation i.e. 41.6 mmol h⁻¹ g_{cat}⁻¹ due to large number of photo-excitons utilized for oxidation reactions through hole (h⁺) with S²⁻, SO₄²⁻ and H₂O to generate H⁺ ions, subsequently reduction of H⁺ with electrons (e⁻) to generate H₂ gas. Further, at lower shell thickness light transmission to core is effective but photo-excitons recombination is predominant thus lower efficiency. Similarly, higher shell thicknesses opaque layer hinders intense of light penetration, results in lesser photo-excitons utilized for reaction. The poor performance of pristine Cu₂S and TiO₂ is attributed to rate of photo-excitons recombination is faster than utilization [31,67,72]. These results are in-line with TEM images and UV-vis spectrum of photocatalysts (vide supra).

Domen et al. [67], investigated the effect of shell thickness on the core surface to conclude that shell thickness of 3–20 nm range is optimum for enhanced photocatalytic H₂ production. Xu et al. [73], also reported metal@TiO₂ (where metal = Au, Pd, and Pt) hierarchical nanohybrid with tunable ultrathin shell exhibited enhanced H₂ production activity. Lakshmana Reddy et al. [32], reported superior photocatalytic H₂ generation utilizing CdS/ZnS core-shell material and concluded that optimization of core diameter and shell thickness significantly affects the process efficiency. Recent report reveals that optimal shell thickness (TiO₂ or NiO) in CdS/TiO₂ and CdS/NiO core-shell photocatalyst accelerates the reaction efficiency besides inhibition of photo-corrosion [30,31].

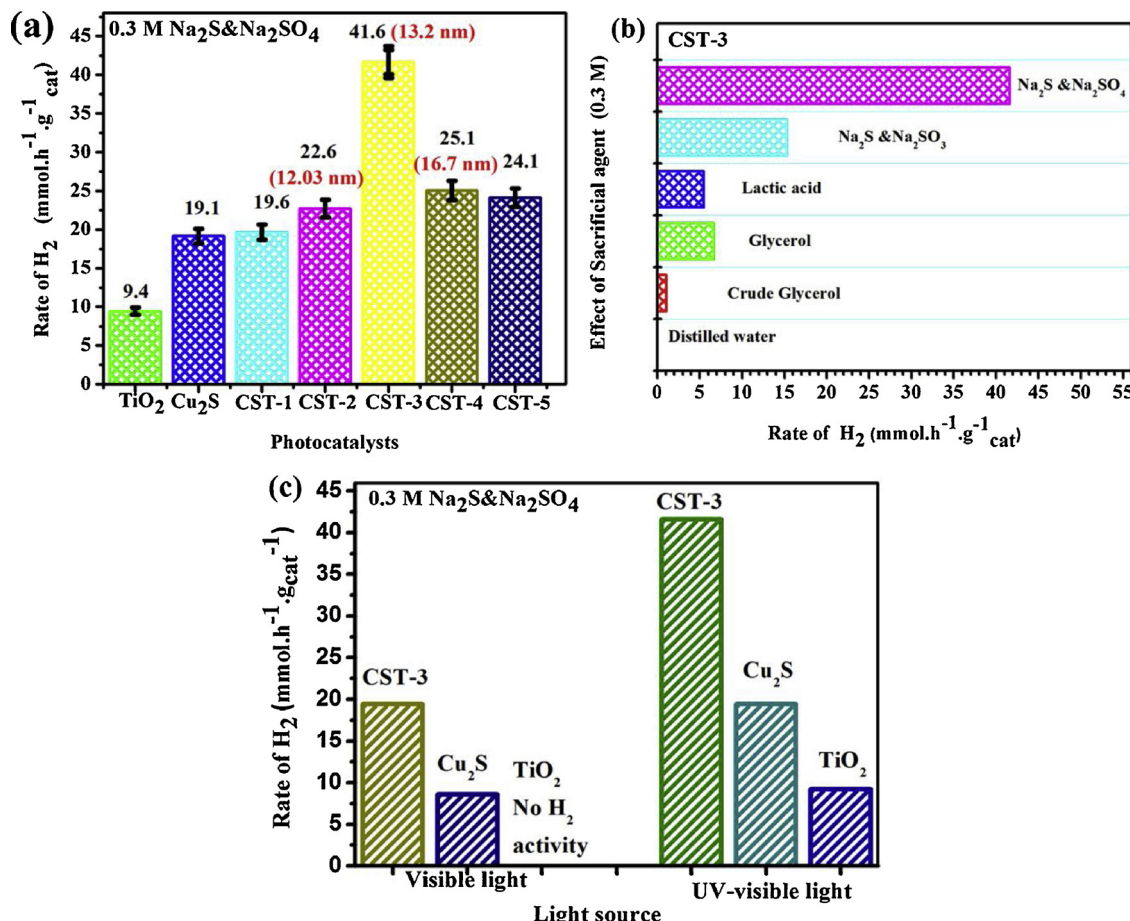


Fig. 9. Photocatalytic activity of Cu₂S@TiO₂ core-shell catalysts under UV-vis light irradiation. (a) optimization of TiO₂ (0.01M to 0.08M) concentration in shell thickness (b) effect of sacrificial agents (c) comparison of core-shell and pristine photocatalysts (CST-3, Cu₂S, TiO₂) under UV-vis light and visible light irradiation.

3.3.2. Effect of sacrificial reagents

A range of sacrificial agents such as alcohols, acids, amines, hydrocarbons and sulphur containing inorganic compounds were usually added at lower quantities into water to enhance the H⁺ generation during oxidation reaction which is essential step for H₂ production as part of photocatalytic process [31,74]. Hence, in the present work, CST-3 photocatalyst evaluated with distilled water, equal molar concentration of alcohol, acid and two types of sulphur containing inorganic compounds. Fig. 9(b) shows rate of H₂ production against different sacrificial agents in the following order: Na₂S&Na₂SO₄ > Na₂S&Na₂SO₃ > Glycerol > Lactic acid > crude glycerol. The highest activity of Na₂S&Na₂SO₄ is ascribed to its higher electro negativity hence better adsorption on catalyst surface and effective oxidation of water into H⁺ ions in-turn H₂ gas production. The lower performance of alcohol and acids are attributed to relatively poor adsorption and electron donating nature. The crude glycerol showed lowest performance due to mixture of lower and higher alcohols besides intermediates that have varied adsorption and electron donating nature that drastically affects the catalytic activity. The above results reveal that electron negativity of sacrificial agents facilitated *in-situ* generation of H⁺ ions and suppress the charge carrier recombination. Lakshmana Reddy et al. [23,30], examined the effect of sacrificial agents such as primary, secondary and tertiary alcohols and found that glycerol having abundant –OH groups readily generated H⁺ ions in aqueous solution using Cu/Ag-TiO₂ nanotubes as photocatalyst.

3.3.3. Effect of light source

The photocatalytic performance of tailor-made catalysts has been tested under different light sources viz., solar light, simulated solar

light/UV-vis light, visible light, monochromatic UV or vis light respectively [75]. In order to delineate the potential role of core (Cu₂S) and shell (TiO₂) in core-shell (Cu₂S@TiO₂) photocatalyst experiments were performed in aqueous solution of 0.3 M Na₂S and Na₂SO₄ under light irradiation using solar simulator with UV cut-off filter (visible light) and no UV filter (UV-vis light). Fig. 9(c) shows photocatalytic H₂ generation using CST-3 (41.6 mmol h⁻¹ g⁻¹cat) and Cu₂S (19.1 mmol nh⁻¹ g⁻¹) under UV-vis light is about two folds higher than visible light irradiation. Whereas under visible light CST-3 (19.4 mmol nh⁻¹ g⁻¹) and Cu₂S (8.6 mmol h⁻¹ g⁻¹cat) displayed about two fold enhanced H₂ generation. In comparison with DR UV-vis spectra (vide supra), the higher activity of core-shell is attributed to Cu₂S in core generated plenty of photo-excitons that can be activated under UV and visible spectrum instead of visible alone. On the other hand, pristine TiO₂ (band gap 3.2 eV) catalyst generated H₂ under UV-vis light and no activity under visible light due to large band gap that can generate excitons only under UV spectrum. In our recent studies, we have reported the synthesis of CdS-NiO and CdS-TiO₂ core-shell photocatalysts and compared their photocatalytic H₂ generation [30,31]. The hierachal photocatalyst showed higher H₂ efficiency compared to pristine materials due to the presence of shell material that has protected the core from photo-corrosion and played a key role for enhanced H₂ production [69].

3.3.4. Time on stream, reusability and recyclability tests of Cu₂S@TiO₂ photocatalyst

In order to explore the real-time potential of the efficient photocatalyst for H₂ generation, test has been conducted to evaluate its performance for prolonged time of utilization, repeated use with fresh

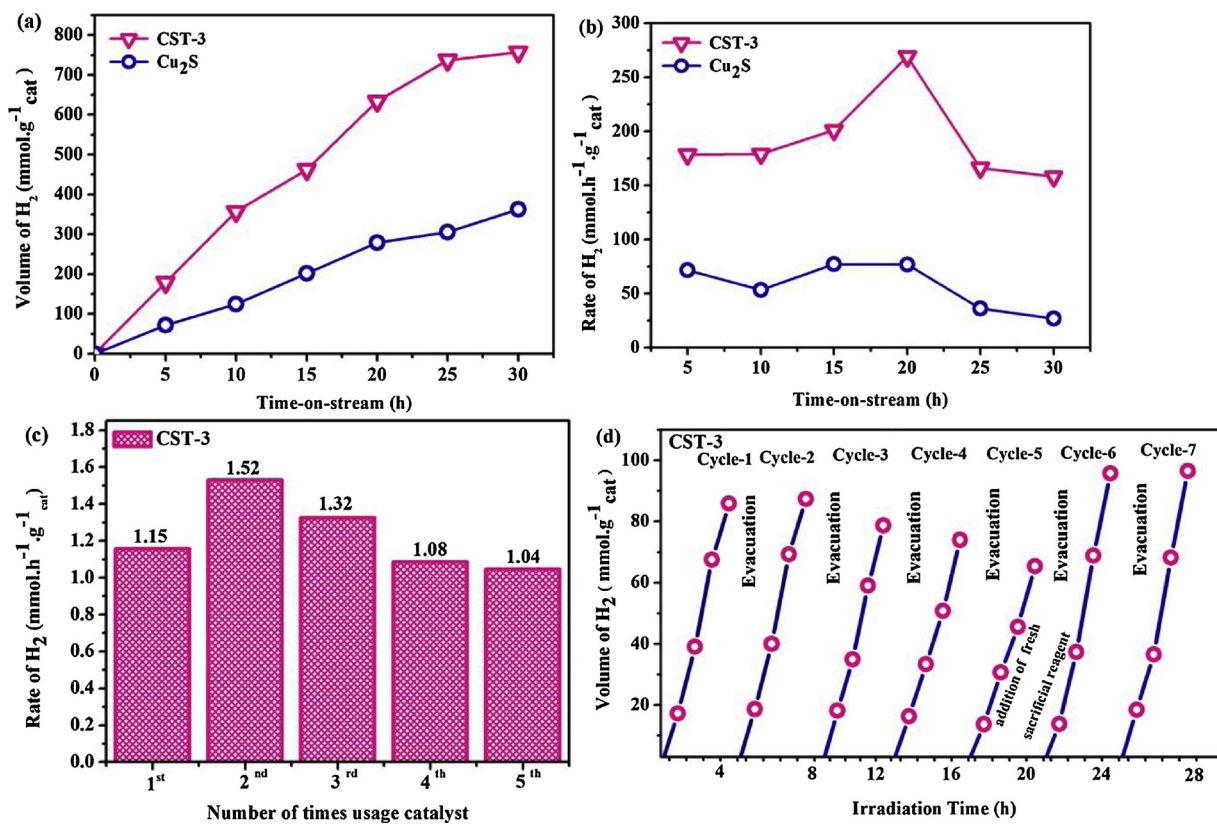


Fig. 10. Performance of CST-3 core-shell photocatalyst (a) Time-on-stream (b) stability (c) reusability (d) Recyclability.

reaction solution and batch experiments performed with same solution with evacuation of generated gas at periodic time intervals [76]. At first, time-on-stream studies were performed continuously for 30 h using pristine Cu₂S and CST-3 dispersed in aqueous solution of 0.3 M Na₂S and Na₂SO₄ under simulated solar light irradiation. Fig. 10(a) displays volume of H₂ generated at 5 h interval and found to increase with irradiation time. In Fig. 10(b) the rate of H₂ evolution linearly increased with time and shows highest value for 20 h and fall-down in activity of ~20% and then stabilize to the similar value for CST-3 catalyst. On the other hand, Cu₂S catalyst displayed about 3 folds lower performance and slight decline in activity noticed for longer irradiation time. The increase in rate of H₂ production for CST-3 is attributed to stabilization of photocatalytic process under experimental conditions and effective release of H₂ gas from reaction medium. However, decline in activity is observed at 25 h and later is due to decrease in concentration of sacrificial agents as it undergoes irreversible oxidation and its intermediates may dramatically affect the catalytic process. The above results indicate that CST-3 exhibited excellent stability with time-on-stream performance for photocatalytic H₂ generation. Lakshmana Reddy et al. [32], explained the stability of core-shell CdS/ZnS photocatalyst under visible LED light for 100 h and 20 h for visible light irradiation. A slight decline in rate of H₂ production after prolonged usage attributed to concentration of sulphide and sulphate ions in reaction solution.

The catalyst reusability tests were carried out under optimized experimental conditions using CST-3 catalyst under simulated solar light irradiation. The catalyst was separated from reaction medium by centrifugation after 4 h of photocatalytic experiments and gas analysis. The separated catalyst was re-suspended into fresh sacrificial agent solution and performed experiments for another 4 h. The same procedure was repeated for 3 more times and rate of H₂ generation in each cycle is displayed in Fig. 10(c). The increase in catalytic performance observed in 2nd and 3rd cycles attributed to well stabilization of catalyst with sacrificial agents for physical adsorption process. Further, decrease and

stable activity in 4th and 5th cycle is observed due to partial masking of catalytic active sites by reaction intermediates. Similarly, MoS₂, Au@MoS₂ and Au@MoS₂-ZnO photocatalysts showed excellent stability for 8 reusability cycles [77].

The recyclability tests were executed for CST-3 under optimized conditions. At first cycle, fresh catalyst and reaction solution were subjected to light irradiation for 4 h and volume of H₂ generated was analyzed and quantified every one hour. In second cycle, the experimental set-up was used after careful evacuation and purged with nitrogen gas to simulate inert atmosphere. Similar procedure was repeated till 5th cycle, whereas fresh solution of 0.3 M sacrificial agent was added into the reactor, 6th and 7th cycle experiments were performed and generated gas was analysed and quantified as per the standard protocol (vide supra). Fig. 10 (d) displayed volume of H₂ generation using CST-3 catalyst and light irradiation period 4 h in each cycle and repeated for seven cycles. It is evident that slight decrease in activity during 3rd, 4th and 5th cycles attributed to decrease in concentration of sulphide and sulphate ions present in solution and regained in performance during 6th and 7th cycle is due to addition of fresh sacrificial agents. Recently Zhang et al. was reports CdS/Titanate nanocomposite for seven cycles each cycle have 12 h continuous irradiation, it was shows good stability [78].

Further, the crystal structure of the fresh and used catalyst was examined by XRD and results are depicted in Fig. 11. It shows that both have similar patterns confirming that CST-3 is highly stable. Further XPS analysis of used catalyst is shown in Fig. 12 (a,b,c and d). The experimental data well matched with fresh catalyst (Fig. 6) there is a slight shift in Ti spectra attributed to Ti-O and Ti-H₂O in Cu₂S@TiO₂ core-shell material. The above results strongly suggest that CST-3 is a stable photocatalyst.

The type of reactor, light source, volume of reaction solution, amount of catalyst etc varies from one laboratory to another. Hence, calculation of reaction efficiency as common parameter enable researchers to compare efficiency of different materials carried out in

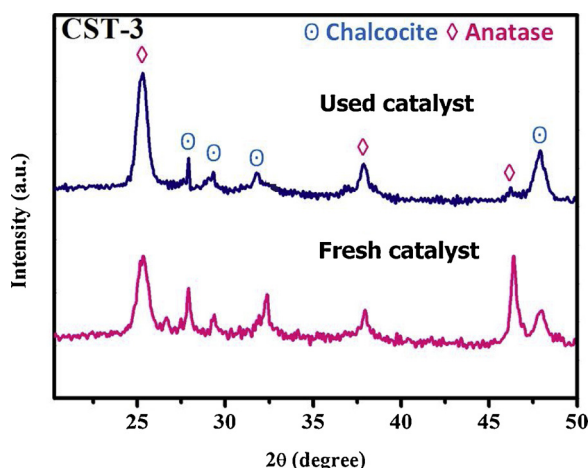


Fig. 11. XRD pattern of fresh and used CST-3 core-shell photocatalyst.

same or different labs. The UV-vis light to H₂ energy conversion were calculated for pristine and the core-shell catalysts are listed in Table 1, where CST-3 showed higher UV-vis light to H₂ conversion efficiency of 10.3% [69] (calculations details are given in the supporting information S3). In addition, quantum efficiency was calculated for CST-3, which is found to be 46.6% (for details see supplementary information S4), under solar light irradiation (1.5 G air mass filter with mean wavelength 768.6 nm) with the rate of H₂ generation as 227 $\mu\text{mol h}^{-1} \text{g}_{\text{cat}}^{-1}$. Moreover, calculated the apparent quantum efficiency of CST-3 is 48.29% (see supplementary information) using air mass filter (1.5 G with mean wavelength 768.6 nm) under solar light irradiation, where the volume of H₂ generation was 771 $\mu\text{mol g}_{\text{cat}}^{-1}$. Zhukovskyi et al. [12],

Table 1

Comparison of photocatalyst for H₂ production and UV-vis light to H₂ conversion efficiency.

S. No.	Photocatalysts	H ₂ generation ($\text{mmol h}^{-1} \text{g}_{\text{cat}}^{-1}$)	UV-vis light ^a to H ₂ production efficiency (%)
1	Cu ₂ S	19.1	4.8
2	TiO ₂	9.2	2.27
3	CST -1	19.6	4.9
4	CST -2	22.6	5.6
5	CST -3	41.6	10.3
6	CST -4	25.1	6.2
7	CST -5	24.1	6.0

Bold values highlight maximum H₂ generation ($\text{mmol h}^{-1} \text{g}_{\text{cat}}^{-1}$) & UV-vis light to H₂ production efficiency (%).

^a UV-vis light intensity = 404 mW/cm².

also calculated apparent quantum efficiency using the reported formula for Ni nanoparticles deposited CdS nanosheets and achieved high apparent quantum efficiency of 25%. Recently Xia et al. [79], reported TiO_{2-x}/MCF composite with a higher quantum yield 46% at 1.5 G air mass filter at the mean wavelength of 584.6 nm. Recently our research group reports developed CdS/ZnS core/shell photocatalyst for high quantum effeciencie is 8.78% at 420 nm wavelength, also explained that optimization of shell thickness plays key a role for improvement photocatalytic H₂ production [32].

3.4. Photocatalytic H₂ generation in H₂S containing wastewater in tank reactor

Photocatalytic H₂ recovery studies were performed under direct natural sunlight irradiation using CST-3 catalyst. Fine tuning of

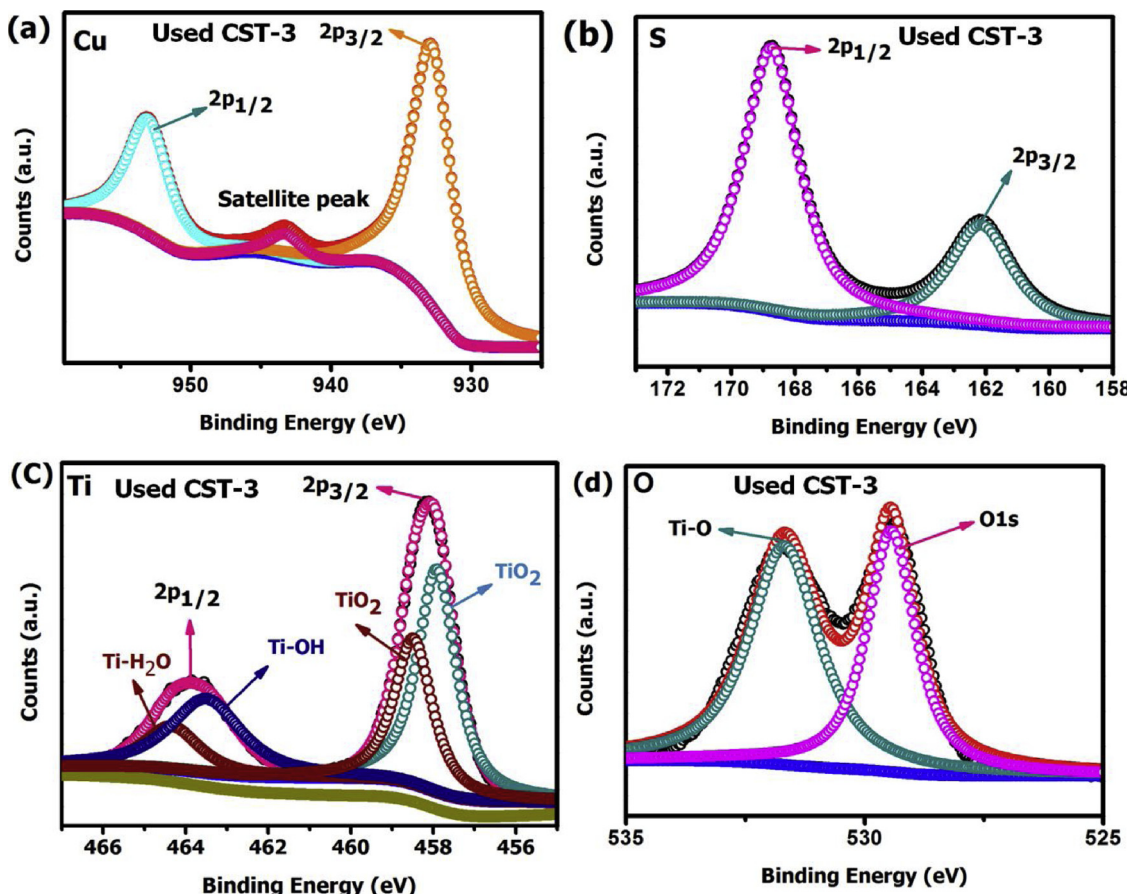


Fig. 12. X-ray photoelectron spectroscopy of used CST-3 catalyst (a) Cu 3d (b) S 2p (c) Ti 2p (d) O 1s.

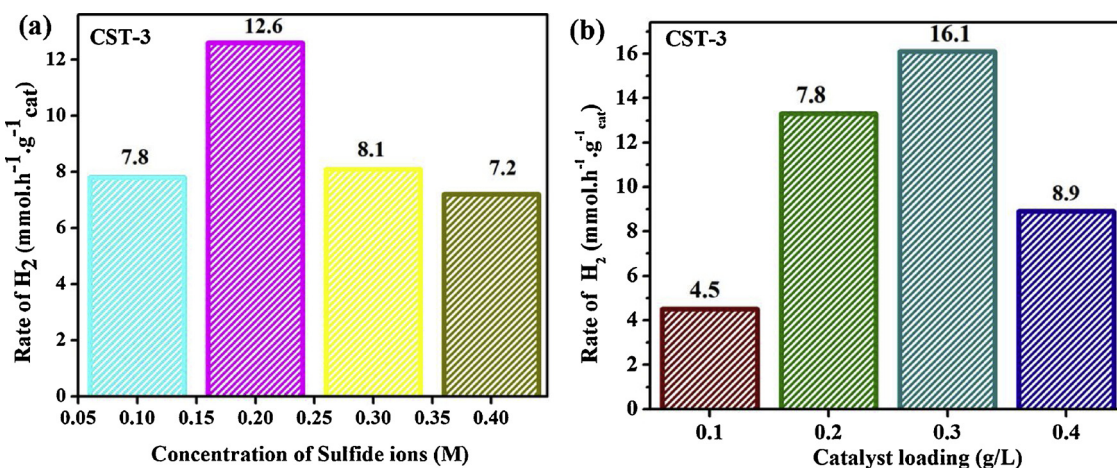


Fig. 13. Photocatalytic H₂ generation from H₂S containing industrial wastewater in tank reactor (a) Effect of sulfite ion concentration (b) Effect of catalyst loading.

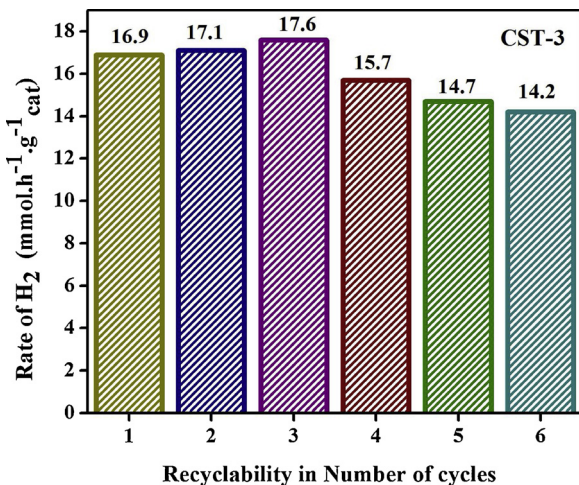


Fig. 14. Photocatalytic H₂ production of the CST-3 for six cycles.

parameters was carried out to optimize sulfite ion concentrations and catalyst loading for recovery of H₂ from an industrial sulfide containing wastewater. The optimized sulfite and catalyst loading was used for recyclability with six cycles.

3.4.1. Effect of sulfite-ion concentration

The concentration of sulphide ion can vary in industrial effluent depends on the process parameters. Based on the experimental data on effect of Na₂S and Na₂SO₄ concentration (vide supra), optimization of sulphide ion concentration is essential to achieve best photocatalytic performance. In the present work, effect of sulfite-ion concentration was studied from 0.1 to 0.4 M. The catalyst loading and average light irradiation used are 0.2 g/L and 1,113 W/m² (calculations available in supporting information S6) respectively. Fig. 13(a) shows the effect of sulfite ion concentration for recovering H₂ gas from the industrial sulfide wastewater. The highest H₂ recovery was found with 0.3M sulfite ion concentration due to the maximum number of hole captured by CST-3 photocatalyst and the reaction solution was in close contact with catalyst surface. Several studies also stated that the smaller or higher amounts of sacrificial reagents may not possible to offer the maximum H₂ generation [47,80,81].

3.4.2. Effect of catalyst loading

Fig. 13(b) shows the amount of catalyst loading for rate of photocatalytic H₂ generation from sulfide wastewater (H₂S). The amount of catalyst loading was studied from 0.1 to 0.4 g/L. The highest H₂

recovery was observed with 0.3 g/L of catalyst loading, ascribed to the abundant catalytic active sites formed on the surface of the CST-3 photocatalyst having better absorption-desorption properties [31,74]. The highest H₂ production was observed at an optimum catalyst loading of 0.3 g/L. It is observed that, at lower catalyst dosage, low catalytic activity is observed and it is proportional to active sites. On the other hand, above the optimum dosage, the opaque solution that significantly limits the light penetration to depth also scatters the photons leads to lower activity. Similar results were also been observed, Ruban et al. [82], reports catalyst loading concentration from 0.1 to 1 g/L amount this 0.5 g/L was optimized.

3.4.3. Reusability of Cu₂S@TiO₂ photocatalyst for sulphide wastewater treatment

Reusability tests were conducted using the optimized sulphite ion concentration (0.3 M), optimized catalyst dosage (0.3 g/L) with an average light irradiation of 127 W/m² (calculation shown in supporting information) for the recovery of H₂ from sulphide wastewater. Fig. 13(a) shows the effect of sulphite ion concentrations on recovery of H₂ from sulphide wastewater. Among the different concentration 0.2 M shows highest H₂ recovery from sulphide wastewater. Fig. 14 shows the reusability of TiO₂/Cu₂S catalyst for 6 cycles and the catalyst was active up to 5 cycles. Due to the core-shell structure, it showed minute charge carrier recombination protecting the core from photocorrosion, suggesting the capability of developed material is scalable for large-scale recovery of H₂ from sulphide wastewater.

3.5. Reaction mechanism of Cu₂S@TiO₂ core-shell photocatalyst

Based on the catalyst characterization data and photocatalytic experimental results, a plausible mechanism is projected for H₂ generation for pristine Cu₂S and Cu₂S@TiO₂ core-shell catalyst and displayed in Fig. 15. Based on the optical properties, it is explained that Cu₂S generated photo-excitons by absorbing light in UV-vis spectrum resulted major bulk/surface recombination besides photo-corrosion. Minor electron/hole at the surface involves in-situ oxidation and reduction reactions resulted in H₂ generation. On the other hand CST-3 having core/shell morphology effectively utilized excitons for generation of H⁺ and its reduction to produce H₂ gas. Moreover, excitons recombination is suppressed greater extent and these results are matching with time resolved photoluminescence spectra. Butler et al., reported the reaction mechanism for enhanced photocatalytic activity towards water splitting using inorganic sacrificial agent solution in contact with the CdS/Pt nanohybrid material [83].

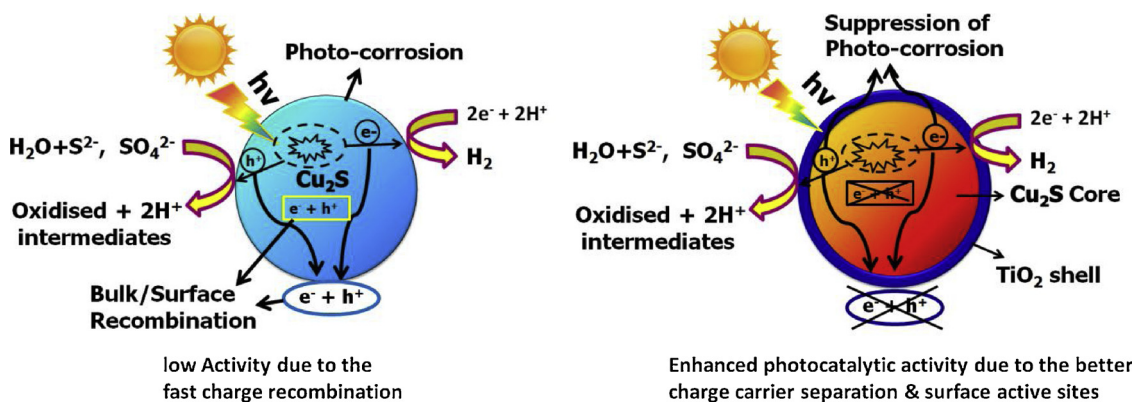


Fig. 15. Plausible reaction mechanism explaining charge carriers transformation from core to shell in $\text{Cu}_2\text{S}@\text{TiO}_2$ photocatalysts.

4. Conclusions

The present study deals with the controlled synthesis of $\text{Cu}_2\text{S}@\text{TiO}_2$ hexagonal and spherical core-shell nanostructures by using structure-directing agent. XRD results confirm chalcocite phase of Cu_2S and anatase TiO_2 . FT-IR revealed the formation of pure CST-3 core-shell nanocomposites via stretching frequencies observed at 632.4, 1628.4, 3445.4 cm^{-1} corresponding to Ti-O, Cu^{+1} and OH functional groups. TEM images revealed hexagonal nanostructured core-shell materials with shell thicknesses ranging from 12.03 to 16.7 nm. UV-vis spectra showed two broad absorption peaks at 450–480 and 500–600 nm, indicating its optical absorption property in the visible spectrum, while XPS and ESR chemical compositions revealed the existence of Cu^{+1} and Ti^{+4} states in Cu_2S and TiO_2 , respectively. Time resolved photoluminescence decay spectra confirmed the prolonged life time of excitons in CST-3 than Cu_2S catalyst.

Photocatalytic H_2 generation of $41.6 \text{ mmol h}^{-1} \text{ g}_{\text{cat}}^{-1}$ using CST-3 was 38% more than that of the Cu_2S core under simulated solar light irradiation. Besides the same catalyst proved stability for time-on-stream experiments. The CST-3 demonstrated a good recyclability for seven cycles and reusability for six cycles, suggesting its promise for practical applications. To the best of our knowledge, this is the first study to report the core-shell catalyst used in the treatment of industrial wastes for clean energy production over $\text{Cu}_2\text{S}@\text{TiO}_2$ core-shell photocatalyst. The enhanced H_2 recovery rate of $16.1 \text{ mmol h}^{-1} \text{ g}_{\text{cat}}^{-1}$ was observed from sulphide wastewater. By fine-tuning of sulphide ion concentration and catalyst dosage, we could achieve good stability for six cycles with a high rate of H_2 production ($17.6 \text{ mmol h}^{-1} \text{ g}_{\text{cat}}^{-1}$) using $\text{Cu}_2\text{S}@\text{TiO}_2$ core-shell photocatalyst.

Acknowledgments

Financial support (Grant Application No.103/227/2014-NT) from Ministry of New and Renewable Energy (MNRE), India is gratefully acknowledged. Authors thankful to RUSA (VV University), MHRD, Govt. of India for providing infrastructural facilities.

Appendix A. Supplementary data

Supplementary material related to this article can be found, in the online version, at doi:<https://doi.org/10.1016/j.apcatb.2019.04.090>.

References

- [1] N.S. Chaudhari, A.P. Bhirud, R.S. Sonawane, L.K. Nikam, S.S. Warule, V.H. Rane, B.B. Kale, Green Chem. 13 (2011) 2500–2506, <https://doi.org/10.1039/c1gc15515f>.
- [2] A.P. Bhirud, S.D. Sathaye, R.P. Waichal, J.D. Ambekar, C.-J. Park, B.B. Kale, Nanoscale 7 (2015) 5023–5034, <https://doi.org/10.1039/C4NR06435F>.
- [3] V. Preethi, S. Kanmani, Int. J. Hydrogen Energy 37 (2012) 18740–18746, <https://doi.org/10.1016/j.ijhydene.2012.09.171>.
- [4] S.K. Apte, S.N. Garaje, G.P. Mane, A. Vinu, S.D. Naik, D.P. Amalnerkar, B.B. Kale, Small 7 (2011) 957–964, <https://doi.org/10.1002/smll.201002130>.
- [5] Y.P. Xie, Z.B. Yu, G. Liu, X.L. Ma, H.-M. Cheng, Energy Environ. Sci. 7 (2014) 1895–1901, <https://doi.org/10.1039/c3ee43750g>.
- [6] Y. Kang, Y. Gong, Z. Hu, Z. Li, Z. Qiu, X. Zhu, P.M. Ajayan, Z. Fang, Nanoscale 7 (2015) 4482–4488, <https://doi.org/10.1039/C4NR07303G>.
- [7] A.P. Bhirud, S.D. Sathaye, R.P. Waichal, L.K. Nikam, B.B. Kale, Green Chem. 14 (2012) 2790, <https://doi.org/10.1039/c2gc35519a>.
- [8] X. Wang, G. Sun, P. Routh, D.-H. Kim, W. Huang, P. Chen, Chem. Soc. Rev. 43 (2014) 7067–7098, <https://doi.org/10.1039/C4CS00141A>.
- [9] C. Sun, J. Zhang, J. Ma, P. Liu, D. Gao, K. Tao, D. Xue, J. Mater. Chem. A 4 (2016) 11234–11238, <https://doi.org/10.1039/C6TA04082A>.
- [10] S. Zhang, X. Yu, F. Yan, C. Li, X. Zhang, Y. Chen, J. Mater. Chem. A 4 (2016) 12046–12053, <https://doi.org/10.1039/C6TA04365H>.
- [11] D. Praveen Kumar, N. Lakshmana Reddy, M. Mamatha Kumari, B. Srinivas, V. Durga Kumari, B. Sreedhar, V. Roddatis, O. Bondarchuk, M. Karthik, B. Neppolian, M.V. Shankar, Sol. Energy Mater. Sol. Cells 136 (2015) 157–166, <https://doi.org/10.1016/j.solmat.2015.01.009>.
- [12] M. Zhukovskiy, P. Tongying, H. Yashan, Y. Wang, M. Kuno, ACS Catal. 5 (2015) 6615–6623, <https://doi.org/10.1021/acscatal.5b01812>.
- [13] Z. Zhang, M. Baek, H. Song, K. Yong, Nanoscale 9 (2017) 5342–5351, <https://doi.org/10.1039/C7NR00336F>.
- [14] K. Maeda, K. Teramura, D. Lu, N. Saito, Y. Inoue, K. Domen, Angewandte Chemie – Int. Edit. 45 (2006) 7806–7809, <https://doi.org/10.1002/anie.200602473>.
- [15] A. Tanaka, K. Teramura, S. Hosokawa, H. Kominami, T. Tanaka, Chem. Sci. 8 (2017) 2574–2580, <https://doi.org/10.1039/C6SC05135A>.
- [16] M.A. Rahman, S. Bazargan, S. Srivastava, X. Wang, M. Abd-Ellah, J.P. Thomas, N.F. Heinig, D. Pradhan, K.T. Leung, Energy Environ. Sci. 8 (2015) 3363–3373, <https://doi.org/10.1039/C5EE01615K>.
- [17] R. Li, Y. Weng, X. Zhou, X. Wang, Y. Mi, R. Chong, H. Han, C. Li, Energy Environ. Sci. 8 (2015) 2377–2382, <https://doi.org/10.1039/C5EE01398D>.
- [18] K. Maeda, A. Xiong, T. Yoshinaga, T. Ikeda, N. Nakamoto, T. Hisatomi, M. Takashima, D. Lu, M. Kanebara, T. Setoyama, T. Teranishi, K. Domen, Angew. Chemie 122 (2010) 4190–4193, <https://doi.org/10.1002/ange.201001259>.
- [19] J. Zhang, Z. Liu, Z. Liu, ACS Appl. Mater. Interfaces 8 (2016) 9684–9691, <https://doi.org/10.1021/acsmami.6b00429>.
- [20] J.-M. Li, H.-Y. Cheng, Y.-H. Chiu, Y.-J. Hsu, Nanoscale 8 (2016) 15720–15729, <https://doi.org/10.1039/C6NR05605A>.
- [21] Z. Li, Z. Zhang, Nanoresearch 11 (2017) 1530–1540, <https://doi.org/10.1007/s12274-017-1769-y>.
- [22] J. Warnan, J. Willkomm, J.N. Ng, R. Godin, S. Prantl, J.R. Durrant, E. Reisner, Chem. Sci. 8 (2017) 3070–3079, <https://doi.org/10.1039/C6SC05219C>.
- [23] N.L. Reddy, S. Kumar, V. Krishnan, M. Sathish, M.V. Shankar, J. Catal. 350 (2017) 226–239, <https://doi.org/10.1016/j.jcat.2017.02.032>.
- [24] A. Gallo, M. Marelli, R. Psaro, V. Gombac, T. Montini, P. Fornasiero, R. Pievo, V.D. Santo, Green Chem. 14 (2012) 330–333, <https://doi.org/10.1039/C2GC16112E>.
- [25] B. Liu, Z. Jin, L. Bai, J. Liang, Q. Zhang, N. Wang, C. Liu, C. Wei, Y. Zhao, X. Zhang, J. Mater. Chem. A 4 (2016) 14204–14212, <https://doi.org/10.1039/C6TA04789K>.
- [26] G. Yang, W. Yan, Q. Zhang, S. Shen, S. Ding, Nanoscale 24 (2013) 12432–12439, <https://doi.org/10.1039/C3nr03462c>.
- [27] H. Wender, R.V. Gonçalves, C.S.B. Dias, M.J.M. Zapata, L.F. Zagonel, E.C. Mendonça, S.R. Teixeira, F. Garcia, Nanoscale 5 (2013) 9310–9316, <https://doi.org/10.1039/C3nr02195e>.
- [28] S.A. Mahapure, P.K. Palei, L.K. Nikam, R.P. Panmand, J.D. Ambekar, S.K. Apte, B.B. Kale, J. Mater. Chem. A 1 (2013) 12835–12840, <https://doi.org/10.1039/C3ta12883k>.
- [29] S.K. Apte, S.N. Garaje, M. Valant, B.B. Kale, Green Chem. 14 (2012) 1455–1462, <https://doi.org/10.1039/C2gc16416g>.
- [30] N.L. Reddy, V.N. Rao, M.M. Kumari, P. Ravi, M. Sathish, M.V. Shankar, Mater. Res. Bull. 101 (2018) 223–231, <https://doi.org/10.1016/j.materresbull.2018.01.043>.
- [31] V.N. Rao, N.L. Reddy, M.M. Kumari, P. Ravi, M. Sathish, B. Neppolian, M.V. Shankar, Mater. Res. Bull. 103 (2018) 122–132, <https://doi.org/10.1016/j.materresbull.2018.01.043>.

- materresbull.2018.03.030.
- [32] N.L. Reddy, V.N. Rao, M.M. Kumari, M. Sathish, S. Muthukonda Venkatakrishnan, Int. J. Hydrogen Energy 43 (2018) 22315–22328, <https://doi.org/10.1016/j.ijhydene.2018.10.054>.
- [33] M. Patil, D. Sharma, A. Dive, S. Mahajan, R. Sharma, Procedia Manuf. 20 (2018) 505–508, <https://doi.org/10.1016/J.PROMFG.2018.02.075>.
- [34] R.J. Vimal Michael, J. Theerthagiri, J. Madhavan, M.J. Umapathy, P.T. Manoharan, RSC Adv. 5 (2015) 30175–30186, <https://doi.org/10.1039/C5RA03621F>.
- [35] L. Sang, Y. Zhao, C. Burda, Chem. Rev. 114 (2014) 9283–9318, <https://doi.org/10.1021/cr400629p>.
- [36] C. Wu, L. Lei, X. Zhu, J. Yang, Y. Xie, Small 3 (2007) 1518–1522, <https://doi.org/10.1002/smll.200700179>.
- [37] J.-H. Park, P. Ramasamy, S. Kim, Y.K. Kim, V. Ahilan, S. Shanmugam, J.-S. Lee, Chem. Commun. 53 (2017) 3277–3280, <https://doi.org/10.1039/C7CC00071E>.
- [38] P. Kar, S. Farsinezhad, X. Zhang, K. Shankar, Nanoscale 6 (2014) 14305–14318, <https://doi.org/10.1039/C4NR05371K>.
- [39] C. Ratanatwanate, A. Bui, K. Vu, K.J. Balkus, J. Phys. Chem. 14 (2011) 6175–6180.
- [40] Y. Zhou, Y. Lei, D. Wang, C. Chen, Q. Peng, Y. Li, Chem. Commun. (Camb.) 51 (2015) 13305–13308, <https://doi.org/10.1039/C5CC05156H>.
- [41] P. Roy, S.K. Srivastava, Mater. Lett. 61 (2007) 1693–1697, <https://doi.org/10.1016/j.matlet.2006.07.101>.
- [42] X. Deng, C. Wang, H. Yang, M. Shao, S. Zhang, X. Wang, M. Ding, J. Huang, X. Xu, Sci. Rep. 7 (2017) 32–36, <https://doi.org/10.1038/s41598-017-04270-y>.
- [43] H.T. Zhang, G. Wu, X.H. Chen, Langmuir 21 (2005) 4281–4282, <https://doi.org/10.1021/la050741j>.
- [44] X. Li, X. He, C. Shi, B. Liu, Y. Zhang, S. Wu, Z. Zhu, Chemsuschem 12 (2014) 3328–3333, <https://doi.org/10.1002/cssc.201402862>.
- [45] Y. Liu, Y. Deng, Z. Sun, J. Wei, G. Zheng, A.M. Asiri, S.B. Khan, M.M. Rahman, D. Zhao, Small. 9 (2013) 2702–2708, <https://doi.org/10.1002/smll.201300197>.
- [46] I. Hwang, M. Baek, K. Yong, ACS Appl. Mater. Interfaces 7 (2015) 27863–27870, <https://doi.org/10.1021/acsmami.5b09442>.
- [47] J. Bharatvaj, V. Preethi, S. Kanmani, Int. J. Hydrogen Energy 43 (2018) 3935–3945, <https://doi.org/10.1016/J.IJHYDENE.2017.12.069>.
- [48] C.-H. Lai, K.-W. Huang, J.-H. Cheng, C.-Y. Lee, B.-J. Hwang, L.-J. Chen, J. Mater. Chem. 20 (2010) 6638, <https://doi.org/10.1039/c0jm00434k>.
- [49] S. Li, K. Yu, Y. Wang, Z. Zhang, C. Song, H. Yin, Q. Ren, Z. Zhu, CrystEngComm. 15 (2013) 1753, <https://doi.org/10.1039/c2ce26692j>.
- [50] H.G. Yang, C.H. Sun, S.Z. Qiao, J. Zou, G. Liu, S.C. Smith, H.M. Cheng, G.Q. Lu, Nature 453 (2008) 638–641, <https://doi.org/10.1038/nature06964>.
- [51] M. El-Maazawi, A.N. Finken, A.B. Nair, V.H. Grassian, J. Catal. 191 (2000) 138–146, <https://doi.org/10.1006/jcat.1999.2794>.
- [52] M. Salavati-Niasari, E. Esmaili, M. Sabet, J. Clust. Sci. 24 (2013) 799–809, <https://doi.org/10.1007/s10876-013-0572-2>.
- [53] W. Du, L. Liao, L. Yang, A. Qin, A. Liang, Sci. Rep. 7 (2017) 1–12, <https://doi.org/10.1038/s41598-017-10904-y>.
- [54] V. Augugliaro, S. Coluccia, V. Loddo, L. Marchese, G. Martra, L. Palmisano, M. Schiavello, Appl. Catal. B 20 (1999) 15–27, [https://doi.org/10.1016/S0926-3373\(98\)00088-5](https://doi.org/10.1016/S0926-3373(98)00088-5).
- [55] M.C. Tsai, J.Y. Lee, P.C. Chen, Y.W. Chang, Y.C. Chang, M.H. Yang, H.T. Chiu, I.N. Lin, R.K. Lee, C.Y. Lee, Appl. Catal. B 147 (2014) 499–507, <https://doi.org/10.1016/j.apcatb.2013.09.033>.
- [56] Q. Cao, R. Che, N. Chen, Appl. Catal. B 162 (2015) 187–195, <https://doi.org/10.1016/j.apcatb.2014.06.052>.
- [57] Y. Liu, Y. Deng, Z. Sun, J. Wei, G. Zheng, A.M. Asiri, S.B. Khan, M.M. Rahman, D. Zhao, Small 9 (2013) 2702–2708, <https://doi.org/10.1002/smll.201300197>.
- [58] Y. Lv, J. Chen, R.K. Zheng, J. Song, T. Zhang, X. Li, X. Shi, L. Chen, Sci. Rep. 5 (2015) 1–8, <https://doi.org/10.1038/srep16291>.
- [59] Z. Khan, M. Khannam, N. Vinothkumar, M. De, M. Qureshi, J. Mater. Chem. 22 (2012) 12090, <https://doi.org/10.1039/c2jm31148h>.
- [60] S.C. Riha, S. Jin, S.V. Baryshev, E. Thimsen, G.P. Wiederrecht, A.B.F. Martinson, ACS Appl. Mater. Interfaces 5 (2013) 10302–10309, <https://doi.org/10.1021/am403225e>.
- [61] Z. Li, Z. Zhang, Nano Res. 11 (2018) 1530–1540, <https://doi.org/10.1007/s12274-017-1769-y>.
- [62] M. Li, R. Zhao, Y. Su, Z. Yang, Y. Zhang, Nanoscale 8 (2016) 8559–8567, <https://doi.org/10.1039/c5nr06908d>.
- [63] S. Liu, N. Zhang, Z.-R. Tang, Y.-J. Xu, ACS Appl. Mater. Interfaces 4 (2012) 6378–6385, <https://doi.org/10.1021/am302074p>.
- [64] D. Praveen Kumar, N. Lakshmana Reddy, B. Srinivas, V. Durgakumari, V. Roddatis, O. Bondarchuk, M. Karthik, Y. Ikuma, M.V. Shankar, Sol. Energy Mater. Sol. Cells 146 (2016) 63–71, <https://doi.org/10.1016/J.SOLMAT.2015.11.030>.
- [65] S. Wang, S. Yang, Mater. Sci. Eng. C 16 (2001) 37–40, [https://doi.org/10.1016/S0928-4931\(01\)00296-X](https://doi.org/10.1016/S0928-4931(01)00296-X).
- [66] S. Wang, Q. Huang, X. Wen, X. Li, S. Yang, T.H. Kong, C.W. Bay, Phys. Chem. Chem. Phys. 4 (2002) 3425–3429, <https://doi.org/10.1039/b201561g>.
- [67] N. Nakamoto, H. Ohtsuka, T. Ikeda, K. Maeda, D. Lu, M. Kanehara, K. Teramura, T. Teranishi, K. Domen, Nanoscale 1 (2009) 106–109, <https://doi.org/10.1039/b9nr00186g>.
- [68] A. Pal, S. Srivastava, R. Gupta, S. Sapra, Phys. Chem. Chem. Phys. 15 (2013) 15888–15895, <https://doi.org/10.1039/c3cp51834e>.
- [69] S. Rawalekar, S. Kaniyankandy, S. Verma, H.N. Ghosh, J. Phys. Chem. C 3 (2010) 1460–1466.
- [70] X. Ma, K. Zhao, H. Tang, Y. Chen, C. Lu, W. Liu, Y. Gao, H. Zhao, Z. Tang, Small 10 (2014) 4664–4670, <https://doi.org/10.1002/smll.201401494>.
- [71] J. Yu, L. Qi, M. Jaroniec, J. Phys. Chem. C 114 (2010) 13118–13125, <https://doi.org/10.1021/jp104488b>.
- [72] H.J. Yun, H. Lee, N.D. Kim, D.M. Lee, S. Yu, J. Yi, ACS Nano 5 (2011) 4084–4090, <https://doi.org/10.1021/mn2006738>.
- [73] N. Zhang, S. Liu, X. Fu, Y.-J. Xu, J. Phys. Chem. C 115 (2011) 9136–9145, <https://doi.org/10.1021/jp2009989>.
- [74] D.P. Kumar, M.V. Shankar, M.M. Kumari, G. Sadanandam, B. Srinivas, V. Durgakumari, Chem. Commun. 49 (2013) 9443–9445, <https://doi.org/10.1039/c3cc44742a>.
- [75] D.J. Martin, K. Qiu, S.A. Shevlin, A.D. Handoko, X. Chen, Z. Guo, J. Tang, Angew. Chemie 126 (2014) 9394–9399, <https://doi.org/10.1002/ange.201403375>.
- [76] P. Ravi, V. Navakoteswara Rao, M. Sathish, Int. J. Hydrogen Energy 43 (2018) 3976–3987, <https://doi.org/10.1016/J.IJHYDENE.2017.08.213>.
- [77] S. Guo, X. Li, J. Zhu, T. Tong, B. Wei, Small 12 (2016) 5692–5701, <https://doi.org/10.1002/smll.201602122>.
- [78] Y. Zhang, Y. Tang, X. Liu, Z. Dong, H.H. Hng, Z. Chen, Small 7 (2013) 996–1002, <https://doi.org/10.1002/smll.201202156>.
- [79] M. Xing, J. Zhang, B. Qiu, B. Tian, M. Anpo, M. Che, Small 11 (2015) 1920–1929, <https://doi.org/10.1002/smll.201403056>.
- [80] X. Hao, Y. Wang, J. Zhou, Z. Cui, Y. Wang, Z. Zou, Appl. Catal. B 221 (2018) 302–311, <https://doi.org/10.1016/J.APCATB.2017.09.006>.
- [81] V. Preethi, S. Kanmani, Int. J. Hydrogen Energy 43 (2018) 3920–3934, <https://doi.org/10.1016/j.ijhydene.2017.11.006>.
- [82] P. Ruban, K. Sellappa, Energy 73 (2014) 926–932, <https://doi.org/10.1016/J.ENERGY.2014.06.107>.
- [83] N. Buehler, K. Meier, J.F. Reber, J. Phys. Chem. 88 (1984) 3261–3268, <https://doi.org/10.1021/j150659a025>.